Monte Carlo Simulation of Two-Component Bilayers: DMPC/DSPC Mixtures*

István P. Sugár,[#] Thomas E. Thompson,[§] and Rodney L. Biltonen[§]
[#]Departments of Biomathematical Sciences and Physiology/Biophysics, Mount Sinai School of Medicine, New York, New York 10029 and [§]Department of Biochemistry and Molecular Genetics, University of Virginia Health Sciences Center, Charlottesville, Virginia 22908

ABSTRACT In this paper, we describe a relatively simple lattice model of a two-component, two-state phospholipid bilayer. Application of Monte Carlo methods to this model permits simulation of the observed excess heat capacity versus temperature curves of dimyristoylphosphatidylcholine (DMPC)/distearoylphosphatidylcholine (DSPC) mixtures as well as the lateral distributions of the components and properties related to these distributions. The analysis of the bilayer energy distribution functions reveals that the gel–fluid transition is a continuous transition for DMPC, DSPC, and all DMPC/DSPC mixtures. A comparison of the thermodynamic properties of DMPC/DSPC mixtures with the configurational properties shows that the temperatures characteristics of the configurational properties correlate well with the maxima in the excess heat capacity curves rather than with the onset and completion temperatures of the gel–fluid transition. In the gel–fluid coexistence region, we also found excellent agreement between the threshold temperatures at different system compositions detected in fluorescence recovery after photobleaching experiments and the temperatures at which the percolation probability of the gel clusters is 0.36. At every composition, the calculated mole fraction of gel state molecules at the fluorescence recovery after photobleaching threshold is 0.34 and, at the percolation threshold of gel clusters, it is 0.24. The percolation threshold mole fraction of gel or fluid lipid depends on the packing geometry of the molecules and the interchain interactions. However, it is independent of temperature, system composition, and state of the percolating cluster.

INTRODUCTION

The thermodynamic parameters of DMPC/DSPC bilayers have been examined experimentally by a number of methods including differential scanning calorimetry (Mabrey and Sturtevant, 1976; van Dijck et al., 1977), dilatometry (Wilkinson and Nagle, 1979), neutron scattering (Knoll et al., 1981), NMR (Lu et al., 1995; Sankaram and Thompson, 1992), ESR (Sankaram et al., 1992), Raman spectroscopy (Mendelsohn and Maisano, 1978), and Fourier transformed infrared spectroscopy (Brumm et al., 1996). The structural characteristics of the fluid and gel coexistence region have been examined experimentally in the mixed systems by FRAP (Vaz et al., 1989; Schram et al., 1996), fluorescence spectroscopy (Piknova et al., 1996), and ESR spectroscopy (Sankaram et al., 1992). These studies have established that DMPC/DSPC forms nonideal mixtures exhibiting positive deviations from ideality. The miscible type phase diagram has a broad gel–fluid coexistence region bordered by solidus and liquidus lines. The positive deviations from ideality imply that the minor phase forms small clusters in a continuum of the major phase (Von Dreele, 1978). However, the clusters are too small to be detectable directly (Pedersen et al., 1996; Sankaram et al., 1992).

DMPC/DSPC two-component bilayers have been investigated theoretically using the phenomenological theory of regular fluids (Ipsen and Mouritsen, 1988; Brumbaugh et al., 1990; Brumbaugh and Huang, 1992). Von Dreele (1978) used the statistical mechanical description of two-component mixtures to calculate the solidus and liquidus lines of the phase diagram, and like–like as well as like–unlike molecular contacts in the all-gel and all-fluid regions. Priest (1980) and Sugar and Monticelli (1985) have calculated the phase diagrams of a series of two-component phospholipid bilayers using the Landau theory of phase transitions. These models, in which the maximum term or mean-field approximations was used, did not provide information about the lateral distribution of the bilayer components, however.

Monte Carlo methods (Jan et al., 1984) have been used to simulate the lateral distribution of the components in the pure gel or fluid phase regions of DMPC/DSPC mixtures assuming one state and two-components. Jørgensen et al., (1993) applied a much more complex model to simulate the phase properties and the lateral distribution of components in the one-phase and the gel–fluid coexistence regions of DMPC/DSPC mixtures. The model assumed that each acyl chain could exist in 10 different states, with the interaction between the two lipid species dependent on the incompatibility of acyl chains of different hydrophobic lengths. Risbo et al. (1995) have studied the type of the gel–fluid transition in the same model by using Monte Carlo simulation in the grand canonical ensemble. Risbo and his coworkers pointed out that the gel–fluid transition in the pure DMPC or DSPC system is a continuous transition but a first order phase transition can be induced when small amounts of another species are mixed in the pure system.

Received for publication 26 May 1998 and in final form 5 January 1999.

*In memory of Dr. Lawrence Garner, M.D.

Abbreviations used: DMPC, dimyristoylphosphatidylcholine; DPPC SUV, dipalmitoylphosphatidylcholine small unilamellar vesicles; DSPC, distearoylphosphatidylcholine; ESR, electron spin resonance; FRAP, fluorescence recovery after photobleaching; MLV, multilamellar vesicles; NMR, nuclear magnetic resonance.

0006-3495/99/04/2099/12 $2.00

The advantage of the Monte Carlo method is that both measurable and currently unmeasurable properties of the system can be simulated. Agreement between the simulated measurable properties and experimental results provides confidence that the unmeasurable quantities are correctly simulated.

In this work, DMPC/DSPC bilayers are described by a two-state, two-component model in canonical ensemble using a set of parameters derived from a limited amount of experimental data. This model is used to simulate the lateral distribution of the components in the pure phase or gel–fluid coexistence regions. After summarizing the bilayer model in the next section, and the steps of the Monte Carlo simulation in the following section, the strategy of parameter fitting is explained in Determination of The Model Parameter. Then, we present and discuss the results of the simulations carried out to investigate the type of the gel–fluid transition at different mole fractions and configurational properties such as the average number of clusters in the minor phase, the size distribution of the clusters, the percolation frequency of the gel and fluid clusters at different temperatures and mole fractions, and the average concentration of DSPC in clusters of different sizes. A comparison is made between the characteristic features of the excess heat capacity curves and properties that are related directly to the bilayer configurations. Then, the conclusions of this paper are summarized.

LATTICE MODEL OF DMPC/DSPC BILAYERS

The model of symmetric bilayers described in this section is a straightforward generalization to two-component bilayers of our two-state model for one-component systems (Sugar et al., 1994, Jerala et al., 1996).

Lattice geometry, states, and configuration

A monolayer of the DMPC/DSPC bilayer is modeled as a triangular lattice of N lattice points (coordination number $z = 6$). Each lattice point is occupied by one acyl chain of either DMPC or DSPC molecules representing component (1) or component (2), respectively. Nearest-neighbor pairs of similar acyl chains are interconnected forming either DMPC or DSPC molecules numbering $N_1/2$ and $N_2/2$, respectively. Every lattice point can exist in two states corresponding to the gel (g) and fluid state (l).

The lattice configuration can be characterized by a square matrix **S** and by a connection vector **c** each containing N elements. Each matrix element S_{ij} represents a lattice point. In accordance with the triangular lattice geometry of the monolayer, the following six matrix elements are the nearest neighbors of the ijth matrix element S_{ij}: $S_{i-1,j-1}$, $S_{i-1,j}$, $S_{i,j-1}$, $S_{i,j+1}$, $S_{i+1,j}$, and $S_{i+1,j+1}$. The possible values of a matrix element 1, 2, 3, and 4 refer to component 1 in the g-state, component 2 in the g-state, component 1 in the l-state and component 2 in the l-state, respectively. Vector **c** lists the lattice positions of the chemically connected pairs of acyl chains, i.e., c_k is the location of the acyl chain connected to the acyl chain in the kth lattice point. The index ij of the **S** matrix elements and the index k of the **c** vector elements are in the following relationship: $k = (j - 1) * \sqrt{N} + i$.

In modeling the transition of one-component phospholipid bilayers, it is not necessary to take into consideration the connections between the acyl chains of the molecules (Jerala et al., 1996). However, in the case of two-component phospholipid bilayers, the connections must be considered to calculate correctly the mixing entropy and percolation threshold concentration of the system. Note that, although by using the independent chain model we could calculate the excess heat capacity curve of DMPC/DSPC mixtures in agreement with the experimental curve, the values of the model parameters were significantly different from those given in Table 1.

Analysis of the configuration matrix **S**, can yield the number of the ith component in mth state (N_i^m) and the number of pairs of nearest neighbor acyl chains (N_{ij}^{mn}), where one of the chains is of component i in state m and the other chain is of component j in state n. Periodic boundary conditions are used to eliminate the effects of the lattice edges (Huang, 1963).

Configurational energy and degeneracy

In this model, E_i^m, the intrachain energy of an acyl chain of component i in state m, is assumed constant and independent of location and orientation of the rotational isomers in the acyl chain. The degeneracy of the energy level of component i in state m is f_i^m. E_{ij}^{mn} is the interaction energy between component i in state m and component j in state n with a degeneracy f_{ij}^{mn}. Only nearest-neighbor interactions between the lattice points are considered because van der Waals interactions between the acyl chains are short-range. (Long-range dipole–dipole interactions between the molecules were originally incorporated into our model. However, in the case of DMPC/DSPC mixtures the effect of the dipole–dipole interaction on the calculated excess heat capacity curves was negligibly small.)

The energy of one layer of the bilayer in configuration **S** is

$$\begin{aligned} E(\mathbf{S}) = {} & E_1^g N_1^g + E_1^l N_1^l + E_2^g N_2^g + E_2^l N_2^l \\ & + E_{11}^{gg} N_{11}^{gg} + E_{11}^{gl} N_{11}^{gl} + E_{11}^{ll} N_{11}^{ll} + E_{12}^{gg} N_{12}^{gg} + E_{12}^{gl} N_{12}^{gl} \\ & + E_{21}^{gl} N_{21}^{gl} + E_{12}^{ll} N_{12}^{ll} + E_{22}^{gg} N_{22}^{gg} + E_{22}^{gl} N_{22}^{gl} + E_{22}^{ll} N_{22}^{ll}. \end{aligned} \tag{1}$$

with a degeneracy

$$\begin{aligned} f(\mathbf{S}) = {} & (f_1^g)^{N_1^g} (f_2^g)^{N_2^g} (f_1^l)^{N_1^l} (f_2^l)^{N_2^l} (f_{11}^{gg})^{N_{11}^{gg}} (f_{11}^{gl})^{N_{11}^{gl}} (f_{11}^{ll})^{N_{11}^{ll}} \\ & (f_{12}^{gg})^{N_{12}^{gg}} (f_{12}^{gl})^{N_{12}^{gl}} (f_{21}^{gl})^{N_{21}^{gl}} (f_{12}^{ll})^{N_{12}^{ll}} (f_{22}^{gg})^{N_{22}^{gg}} (f_{22}^{gl})^{N_{22}^{gl}} (f_{22}^{ll})^{N_{22}^{ll}}. \end{aligned} \tag{2}$$

Configurational probability

The probability of configuration **S** in thermodynamic equilibrium is

$$p(\mathbf{S}) = \frac{f(\mathbf{S}) e^{-E(\mathbf{S})/kT}}{Q(N, T, V)} = \frac{e^{-\chi(\mathbf{S})/kT}}{Q(N, T, V)}, \tag{3}$$

TABLE 1 Model parameters of the two-state two-component (DMPC/DSPC) bilayer model

Parameters	(cal/mol-chain)
ΔE_1	3,028
ΔE_2	5,250
w_{11}^{gl}	323.45
w_{22}^{gl}	352.32
w_{12}^{gg}	135
w_{12}^{ll}	80
w_{12}^{gl}	370
w_{12}^{lg}	410
	(cal/mol-chain/deg)
ΔS_1	10.19378
ΔS_2	16.01689

where $Q(N, T, V)$ is the partition function of the canonical ensemble of the lattice model, T is the absolute temperature, and k is the Boltzmann constant. Any change in the number of lipid molecules and bilayer volume associated with the transition is neglected. The function $\chi(\mathbf{S})$ is defined by

$$\chi(\mathbf{S}) = E(\mathbf{S}) - kT \ln f(\mathbf{S}). \tag{4}$$

The configuration-dependent part of this function plays a central role in the Monte Carlo simulation. Equation 4 can be reduced to Eq. 5 to obtain $\bar{\chi}(\mathbf{S})$, the configuration-dependent part of $\chi(\mathbf{S})$

$$\begin{aligned}\bar{\chi}(\mathbf{S}) = {} & N_1^{\mathrm{l}}(\Delta E_1 - T\Delta S_1) + N_2^{\mathrm{l}}(\Delta E_2 - T\Delta S_2) + w_{11}^{\mathrm{gl}} N_{11}^{\mathrm{gl}} \\ & + w_{22}^{\mathrm{gl}} N_{22}^{\mathrm{gl}} + w_{12}^{\mathrm{gg}} N_{12}^{\mathrm{gg}} + w_{12}^{\mathrm{ll}} N_{12}^{\mathrm{ll}} + w_{12}^{\mathrm{gl}} N_{12}^{\mathrm{gl}} \\ & + w_{21}^{\mathrm{gl}} N_{21}^{\mathrm{gl}},\end{aligned} \tag{5}$$

where

$$\Delta E_{\mathrm{i}} = [E_{\mathrm{i}}^{\mathrm{l}} + (z/2)E_{\mathrm{ii}}^{\mathrm{ll}}] - [E_{\mathrm{i}}^{\mathrm{g}} + (z/2)E_{\mathrm{ii}}^{\mathrm{gg}}], \tag{6}$$

$$\Delta S_{\mathrm{i}} = k \ln f_{\mathrm{i}}^{\mathrm{l}} - k \ln f_{\mathrm{i}}^{\mathrm{g}}, \tag{7}$$

$$w_{\mathrm{ij}}^{\mathrm{mn}} = \left[E_{\mathrm{ij}}^{\mathrm{mn}} - \frac{E_{\mathrm{ii}}^{\mathrm{mm}} + E_{\mathrm{jj}}^{\mathrm{nn}}}{2}\right] - kT \ln\left[\frac{f_{\mathrm{ij}}^{\mathrm{mn}}}{\sqrt{f_{\mathrm{ii}}^{\mathrm{mm}} f_{\mathrm{jj}}^{\mathrm{nn}}}}\right]. \tag{8}$$

STEPS IN THE MONTE CARLO SIMULATIONS

Initial configuration

Each simulation starts from either an all-gel or all-fluid state. Initially, component (1) is assigned to the first N_1 lattice points, whereas component (2) is assigned to the remaining N_2 lattice points. Initially, the molecules are similarly oriented (i.e., the acyl chains on the first and second lattice points represent a phospholipid molecule), and, in general, the acyl chains on the $2k - 1$th and $2k$th lattice points are connected (i.e., $c_{2k-1} = 2k$).

Generation of trial configurations

During the Monte Carlo simulation, trial configurations of the two-component phospholipid bilayers are generated by means of three different elementary steps. In one step, the trial configuration is generated by changing the state of a randomly selected acyl chain from gel to fluid or from fluid to gel. This trial configuration generation, the Glauber method (Glauber, 1963), is essential for the simulation of gel-to-fluid transitions of lipid bilayers. In another step, two randomly selected molecules of different lipid components are exchanged. Although this elementary, nonphysical step is different from the Kawasaki (1972) method, in which nearest-neighbor molecules are exchanged, the attainment of the equilibrium of the lateral distribution of the bilayer components is faster (Sun and Sugar, 1997). Finally, a pair of nearest-neighbor molecules are randomly selected. If the positions of the selected acyl chains define the nodes of a rhombus, then one of the chains and the chain on the opposite node are exchanged (Jerala et al., 1996). This exchange involves a rotation of the respective molecules by $\pm 60°$. A series of these elementary reorientations leads to the equilibrium distribution of the orientation of the molecules. Note that, like the exchange of different molecules, the reorientation step results in the lateral movement of the molecules. Thus, a series of reorientation steps is able to drive the system to equilibrium of the lateral distribution of the molecules. However, as mentioned above, the nonphysical steps of exchanging different molecules are also used to substantially accelerate convergence to the equilibrium distribution (Sun and Sugar, 1997).

A trial configuration, $\mathbf{S}_{\mathrm{trial}}$, once generated, is acceptable when the following inequality holds,

$$\mathrm{RAN} \le \exp[-\{\bar{\chi}(\mathbf{S}_{\mathrm{trial}}) - \bar{\chi}(\mathbf{S}_{\mathrm{orig}})\}/kT]. \tag{9}$$

If it is not, the original configuration, $\mathbf{S}_{\mathrm{orig}}$, is retained. In Eq. 9, RAN is a pseudorandom number, distributed homogeneously in the interval (0, 1). This method of decision making drives the system toward thermodynamic equilibrium, the Boltzmann distribution over the configurations, independently of the choice of the initial configuration (Sun and Sugar, 1997).

Defining the Monte Carlo cycle

In a Monte Carlo simulation, a chain of elementary steps generating trial configurations is repeated. During this chain of elementary steps, the Monte Carlo cycle, the system has the opportunity of realizing all of its configurations one time. N elementary steps of local state alteration give the opportunity of realizing any of the 2^N acyl chain states of the lattice. By exchanging different molecules $(N/2)!/[(N_1/2)!\ (N_2/2)!]$, different arrangements of the molecules can be created. Any one of these arrangements can be realized by repeating the elementary steps of exchange of different molecules $N_1/2$ times (or $N_2/2$ times if $N_2 > N_1$).

An acyl chain at the ith lattice point is connected with one of the six nearest-neighbor acyl chains. Assuming independent orientations of the molecules, $3^{N/2}$ is the total number of different orientations in the lattice. In reality, the orientations of the molecules are coupled, and thus the number of possible orientations in the bilayer is much smaller. The probability that any selected lipid molecule has a neighbor that can participate in a reorientation step is 0.75 on a lattice with randomly oriented molecules (Jerela et al., 1996). After $N/2/0.75$ reorientation steps, about 50% of the molecules have an opportunity to change orientation by $+60°$, while the other half of the molecules can change orientation by $-60°$. Each orientation is accessible for each molecule at least once after performing $2(N/2/0.75) = 4N/3$ reorientation steps.

Global state alteration

In principle, the equilibrium distribution of the system is attainable after many Monte Carlo cycles. In practice, however, the system could be trapped during the time of the simulation in one of the energy minima dependent on the initial configuration. Accelerated convergence to the equilibrium distribution can be obtained by incorporating nonphysical, shuffling operations into the algorithm (Sun and Sugar, 1997). We incorporated a shuffling operation at the end of each Monte Carlo cycle, to provide the opportunity of altering the state of every acyl chain from gel to fluid and from fluid to gel.

In our Monte Carlo simulations, we first ran 6000 Monte Carlo cycles and then collected data from the next 6000 cycles to estimate the equilibrium averages of lattice energy, cluster size, number of clusters, and percolation frequencies of gel and fluid clusters (Sugar et al., 1994). After determining the average lattice energy at fifty different temperatures, the excess heat capacity curve was obtained from the numerical derivative of the calculated energy curve. In an alternative method, the variance of the energy at different temperatures was calculated to obtain directly the excess heat capacity curve (Sugar et al., 1994). This method is more time consuming, however, because convergence to the equilibrium value of the energy variance is an order of magnitude slower than convergence to the energy average (Mezei and Beveridge, 1986). In the case of our simulation protocol, the two methods resulted in essentially the same excess heat capacity values.

DETERMINATION OF THE MODEL PARAMETERS

The $\bar{\chi}(\mathbf{S})$ function, Eq. 5, contains 10 unknown model parameters: ΔE_1, ΔE_2, ΔS_1, ΔS_2, w_{11}^{gl}, w_{22}^{gl}, w_{12}^{gg}, w_{12}^{ll}, w_{12}^{gl}, w_{21}^{gl}. The model parameters have been determined by the following strategy. Parameters ΔE_1 and ΔE_2 were estimated by means of the integral of the measured excess heat capacity curves of single component DMPC and DSPC MLV's, respectively. The low and high temperature limits of integration were specified as those temperatures at which the experimental heat capacity curve deviated from the high and low temperature base lines. At the maxima of the calculated

excess heat capacity curves of the one-component systems at the respective measured temperatures of the heat capacity maxima, T_{m1} and T_{m2}, the model parameters should satisfy the following two constraints: $\Delta S_1 \approx \Delta E_1/T_{m1}$ and $\Delta S_2 \approx \Delta E_2/T_{m2}$. These approximate relationships can be derived when the parameters w_{11}^{gl} and w_{22}^{gl} are equal to zero and $2kT_{mi} \ll \Delta E_i$ (see Appendix). In the case of a DSPC bilayer, the above approximation results in an error of about 3% in the value of ΔS_2. The remaining two parameters of the one-component systems, w_{11}^{gl} and w_{22}^{gl}, were estimated by comparing the experimental excess heat capacity at T_{mi} of each one-component system with a series of excess heat capacities calculated at different values of the respective w_{ii}^{gl} parameter. The parameters resulting in a good fit of the entire heat capacity curve are listed in Table 1.

In Table 1, the parameters, $w_{11}^{lg} = 323.45$ cal/mol-chain and $w_{22}^{lg} = 352.32$ cal/mol-chain, are about 20% larger than the value of the parameters obtained from similar analysis of the excess heat capacity curve of DPPC SUV (Sugar et al., 1994; Jerala et al., 1996, Heimburg and Marsh, 1996). The somewhat larger value obtained here is the result of higher cooperativity associated with the gel–fluid transition of MLV as evidenced by the narrower excess heat capacity function.

The positions of the high- and low-temperature peaks in the excess heat capacity curves for the binary mixtures are strongly related to the values of the parameters w_{12}^{gg} and w_{12}^{ll}. In the case of a 60/40 mixing ratio, the calculated low- and high-temperature peaks in the excess heat capacity curves were obtained in agreement with the observed peak positions by assuming $w_{12}^{gg} = 135$ cal/mol-chain and $w_{12}^{ll} = 80$ cal/mol-chain. This result shows that the pure fluid phase is closer to an ideal mixture than the pure gel phase, as expected.

The values of the remaining two parameters, w_{12}^{lg} and w_{12}^{gl} were estimated simultaneously, by comparing the calculated excess heat capacity curve, obtained with different pairs of the parameter values, with the experimental excess heat capacity curve at a mixing ratio of 60/40. In Fig. 1 *A*, the calculated and experimental excess heat capacity curves are shown at a DMPC/DSPC mixing ratio of 60/40. The parameters used in this and all the subsequent simulations are listed in Table 1. In estimating these parameters, it was assumed that the w_{ij}^{mn} parameters are independent of temperature. We note that the method suggested by Ferrenberg and Swendsen (1988) of accelerating multiparameter fitting is not practical in our Monte Carlo simulations because the tabulation of the distribution function of N_1^l, N_2^l, N_{11}^{gl}, N_{22}^{gl}, N_{12}^{gg}, N_{12}^{ll}, N_{12}^{lg}, N_{12}^{gl} in an eight-dimensional matrix requires a prohibitively large memory.

In respect to the reliability of the estimated parameter values, we emphasize the following points.

1. In our model, three parameters are required to describe the heat capacity curve of a pure lipid bilayer: the energy change, ΔE_i, the entropy change, ΔS_i and the parameter, w_{ii}^{gl}. The first is estimated by the integral of the heat capacity curve, and the second is estimated from the energy change and temperature at the position of the maximum of the heat capacity curve, both experimental parameters. The experimental error of the transition enthalpy is less than 10%. Because the error of the temperature measurement is very small, the error of the transition entropy is also less than 10%. The third parameter, w_{ii}^{gl} is the only adjustable parameter and is very robust in terms of precisely defining the height and shape of the heat capacity curve. For example, changes in w_{ii}^{gl} by less than 10% can produce a four-fold change in the maximum value of the heat capacity curve. The experimental error in the maximum value of the excess heat capacity curve is less than 5%.
2. For analysis of the mixed systems, ten parameters are required, six of which are defined by analysis of the two pure systems, whereas the other four were determined by two separate exhaustive searches with a single mixed system. The parameter search was manageable because w_{12}^{gg} and w_{12}^{ll} parameters are largely uncorrelated with w_{12}^{gl} and w_{12}^{lg} parameters as far as their effect on the shapes of the heat capacity curves, and thus, separate exhaustive searches could be made for the values of these two pairs of w parameters. After these four parameters were estimated, their adequacy to reproduce the heat capacity curves for nine mixtures ranging from 10% to 90% DSPC was tested. If satisfactory agreement was achieved, the parameters were assumed to be correct. It should be noted that a change of $\leqslant \pm 5$ cal/mol-chain in any of these four parameters did not alter significantly the shape of the simulated heat capacity curves. It appears that the set of parameters deduced for this system is unique and quite robust.

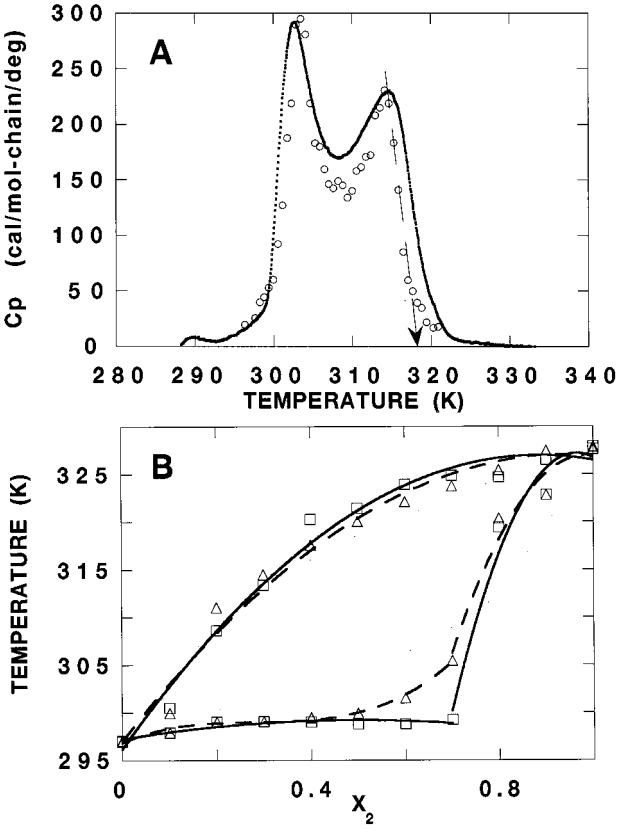

FIGURE 1 Experimental and calculated excess heat capacity curves and phase diagrams of DMPC/DSPC mixtures. (*A*) Excess heat capacity curves. *Dotted line,* experimental excess heat capacity curve of DMPC/DSPC (60/40) mixture; ○, calculated values. All calorimetric scans were performed on a home-made high sensitivity scanning calorimeter (Suurkuusk et al., 1976) at scan rates from 0.1 to 5°C/h. In this scan, the lipid concentration was 20 mM with a scan rate of 5°C/h. To obtain the calculated excess heat capacity, the variance of the lattice energy E was determined at each temperature and then the following equation was used: $C_p \approx C_V = \langle (E - \langle E \rangle)^2 \rangle)/(RT^2N)$ where $R = 2$ cal/mol-chain/deg. The determination of the completion temperature of the gel-to-fluid transition is also shown. A straight line is fitted to the inflection point of the excess heat capacity curve close to the completion of the transition (*dashed line*) and its intercept with the baseline defines the completion temperature (*arrow*). Model parameters are listed in Table 1. (*B*) DMPC/DSPC phase diagrams. The △ and □, representing, respectively, the calculated and experimental onset and completion temperatures of the gel-to-fluid transition at different DSPC mole fractions, were used to construct the solidus and liquidus lines of the phase diagram.

To eliminate finite size effects in our simulations, we choose lattices larger than a minimum size. Above the minimum size, the calculated excess heat capacity is practically independent from the lattice size. After performing simulations at different lattice sizes, the following minimum sizes were obtained: 300 × 300 for DMPC, 50 × 50 for DMPC/DSPC (90/10) mixture, 30 × 30 for DMPC/DSPC (80/20 and 10/90) mixtures, 100 × 100 for DSPC and 20 × 20 for every other mole fraction. By taking into consideration these minimum lattice sizes in the subsequent simulations, the following lattice sizes were used: 350 × 350 for DMPC; 300 × 300 for DSPC; 100 × 100 for DMPC/DSPC mixtures of mixing ratios

10/90, 20/80, 90/10, 80/20; and 40 × 40 for DMPC/DSPC mixtures of mixing ratios 30/70, 40/60, 50/50, 60/40, 70/30.

RESULTS AND DISCUSSION

By using the model parameters listed in Table 1, one can simulate the excess heat capacity curves at different DMPC/DSPC mole fractions. The predictability of various curves is evidenced by the comparison of the observed and calculated temperatures at the maxima of the excess heat capacity curves (Table 2) and by the comparison of the observed and calculated temperatures at the onset and completion of the transition (Fig. 1 *B*). Commonly, the onset and completion temperatures are determined from the experimental heat capacity curves at different mole fractions to construct the solidus and liquidus curves of the phase diagram. The determination of the completion temperature from the excess heat capacity curve is defined in the legend to Fig. 1 *A*.

The type of the transition

The type of the transition can be determined from the distribution function of the fluctuating extensive parameters of the system. The transition is a continuous transition or a first order phase transition if, at the mid-point of the transition, the distribution function is unimodal or bimodal, respectively.

In this work, the bilayer is modeled by a canonical ensemble, in which the internal energy is the only fluctuating extensive variable. At every DMPC/DSPC mole fraction, the simulations show that, with increasing lattice size, the bimodal energy distributions become unimodal (Fig. 2 *A–C*), and thus, in the thermodynamic limit (infinite lattice size) it appears that the gel–fluid transition is a continuous transition. In Fig. 2 *D*, the lattice size, where the bimodal distribution turns into unimodal, is plotted against the mole fraction. It is important to note that this lattice size value is similar to the minimum lattice size, introduced in the previous section.

Risbo et al. (1995) have studied the type of the gel–fluid transition in DMPC/DSPC systems by using Monte Carlo simulation in the grand canonical ensemble. In contrast to our result, in Risbo's system, first-order phase transition can be induced when small amounts of another species are mixed in the pure system, i.e., the equilibrium distribution functions of the DMPC/DSPC mole fraction as well as the lattice energy are bimodal. This means that the initially similar composition of the DMPC/DSPC vesicles becomes very different when equilibrium is attained. We think that the canonical description is more appropriate because, within the time frame of the calorimetric experiments, the exchange of lipids between vesicles practically does not occur. The exchange rate is on the order of many hours to days (Wimley and Thompson, 1990).

Gel-to-fluid transition in DMPC/DSPC mixtures

Fig. 3 *A* and *B* show the temperature dependence of the average number of DMPC and DSPC chains, respectively, in the fluid state for mixtures of different composition. The temperatures at the steepest sections of these sigmoidal melting curves, $T_{N_1^l}$ and $T_{N_2^l}$ are listed in Table 3. There is excellent agreement between these temperatures and the respective peak positions of the calculated excess heat capacity curve (T_{peak1}, T_{peak2}). Because the peak positions of the calculated and experimental heat capacity curves are in close agreement (Table 2), the temperatures of steepest melting of the components of the bilayer can thus be predicted from the experimental heat capacity results.

In Fig. 4, the average number of different nearest-neighbor chains ($\langle N_{11}^{gl}\rangle$, $\langle N_{22}^{gl}\rangle$, $\langle N_{12}^{gg}\rangle$, and $\langle N_{12}^{ll}\rangle$) are calculated as a function of temperature. With increasing temperature, $\langle N_{12}^{gg}\rangle$ decreases, whereas $\langle N_{12}^{ll}\rangle$ increases. The temperatures at the steepest decrease and increase, $T_{N_{12}^{gg}}$ and $T_{N_{12}^{ll}}$ are listed in Table 3. There is, again, excellent agreement between these temperatures and the respective peak positions of the calculated excess heat capacity curves (T_{peak1} and T_{peak2}).

The $\langle N_{11}^{gl}\rangle$, $\langle N_{22}^{gl}\rangle$, $\langle N_{12}^{lg}\rangle$, and $\langle N_{12}^{gl}\rangle$ curves have maxima at temperatures $T_{N_{11}^{gl}}$, $T_{N_{22}^{gl}}$, $T_{N_{12}^{lg}}$, and $T_{N_{12}^{gl}}$, respectively. $T_{N_{11}^{gl}}$ is in agreement with the position of the first peak, T_{peak1}, whereas $T_{N_{12}^{gl}}$ agrees with T_{peak2} in the range of DSPC mole fraction from 0.4 to 1. The position of the maximum of $\langle N_{12}^{lg}(T)\rangle$ is consistently between the peak positions of the excess heat capacity curve at any mole fraction.

Many processes occur in lipid bilayers that may be the result of defects in the packing of the component molecules (see citations of Wimley and Thompson, 1991). These include interbilayer, transbilayer lipid exchange, and membrane permeability of small polar molecules. In the gel–

TABLE 2 Calculated and experimental temperatures at the peaks of the excess heat capacity curves of DMPC/DSPC bilayers at different DSPC mole fractions X_2

X_2*	0.0	0.1	0.2	0.3	0.4	0.5	0.6	0.7	0.8	0.9	1.0
T_{peak1}	297.04	298.92	300.2	302.26	303.77	304.9	307.8	310.4#	—	—	—
T^{exp}_{peak1}	297.04	298.9	299.9	300.9	302.6	304.7	306.0#	304.9#	—	—	—
T_{peak2}	—	—	308.1#	310.4	314.4	316.9	318.9	321.3	324.0	325.6	327.78
T^{exp}_{peak2}	—	—	306.4#	310.0	314.4	318.5	321.0	322.8	324.0	326.0	327.78

*T_{peak1} and T^{exp}_{peak1}, calculated and experimental temperature at the low-temperature peak of the excess heat capacity curve; T_{peak2} and T^{exp}_{peak2}, calculated and experimental temperature at the high-temperature peak of the excess heat capacity curve.

Temperatures at shoulders of the excess heat capacity curves.

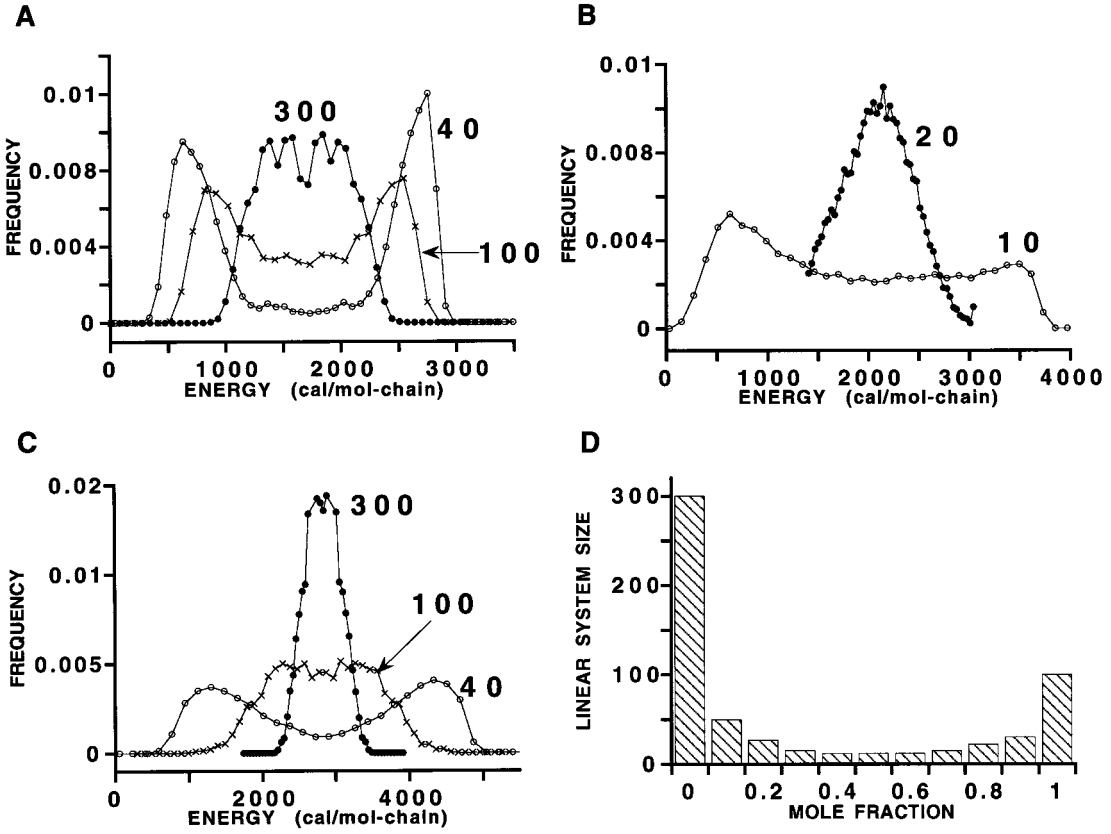

FIGURE 2 Lattice energy distributions. Energy distributions are shown at the following DSPC mole fractions: (*A*) 100/0, (*B*) 70/30, and (*C*) 0/100. Each curve is labeled by the respective linear lattice size. (*D*) The region of linear lattice size where the energy distribution is bimodal is plotted against the DSPC mole fraction.

fluid coexistence region, formation of packing defects is most probable along the gel–fluid interface. In Fig. 4, the sum of $\langle N_{11}^{gl}\rangle$, $\langle N_{22}^{gl}\rangle$, $\langle N_{12}^{lg}\rangle$, and $\langle N_{12}^{gl}\rangle$ is plotted against the temperature ($\times$). This sum should be directly proportional to the total length of the interface between gel and fluid clusters, which has been assumed to be related to the permeability of small polar molecules across the lipid bilayer (Marsh et al., 1976; Cruzeiro-Hansson and Mouritsen, 1988; Clerc and Thompson, 1995).

Lipid compositions in the gel-fluid coexistence region

The mole fraction of DSPC chains in the fluid, X_2^l, and in the gel state regions, X_2^g, can be calculated from the melting curves in Fig. 3 as

$$X_2^l(T) = \frac{\langle N_2^l(T)\rangle}{\langle N^l(T)\rangle} \tag{10}$$

$$X_2^g(T) = \frac{\langle N_2^g(T)\rangle}{\langle N^g(T)\rangle} = \frac{N_2 - \langle N_2^l(T)\rangle}{N - \langle N^l(T)\rangle} \tag{11}$$

where $\langle N^l(T)\rangle = \langle N_1^l(T)\rangle + \langle N_2^l(T)\rangle$.

In Fig. 5 *A* and *B*, the calculated $X_2^l(T)$ and $X_2^g(T)$ curves are shown at different DSPC mole fractions. At low temperatures the composition of the gel clusters is similar to the total composition ($X_2^g \approx X_2$), whereas at high temperatures, the composition in the fluid clusters is similar to the total composition ($X_2^l \approx X_2$). At temperatures where the above approximations fail, the gel-to-fluid transition takes place.

Below the transition temperature of DMPC, the DMPC/DSPC mixtures exist in the gel state (i.e., $X_2^g \approx X_2$). With increasing temperature, primarily DMPC melting takes place first, resulting in a sudden increase of X_2^g. The increase of X_2^g, however, lessens and then starts to decrease at the temperature where DSPC melting becomes more intense.

The situation is just the opposite for the solidification process when DSPC freezing takes place first, resulting in a sudden decrease of X_2^l. The decrease of X_2^l lessens and then starts to increase at the temperature where DMPC freezing becomes more pronounced.

It is important to note that, in a two-component system, the transition is a first-order phase transition if the composition in either the gel (X_2^g) or fluid state region (X_2^l) remains constant when the total mole fraction (X_2) is changed while the temperature is kept constant. This property of the first-order phase transition results in the lever rule, a linear relationship between the mole fraction X_2 and fractional completion of the phase transition. In the DMPC/

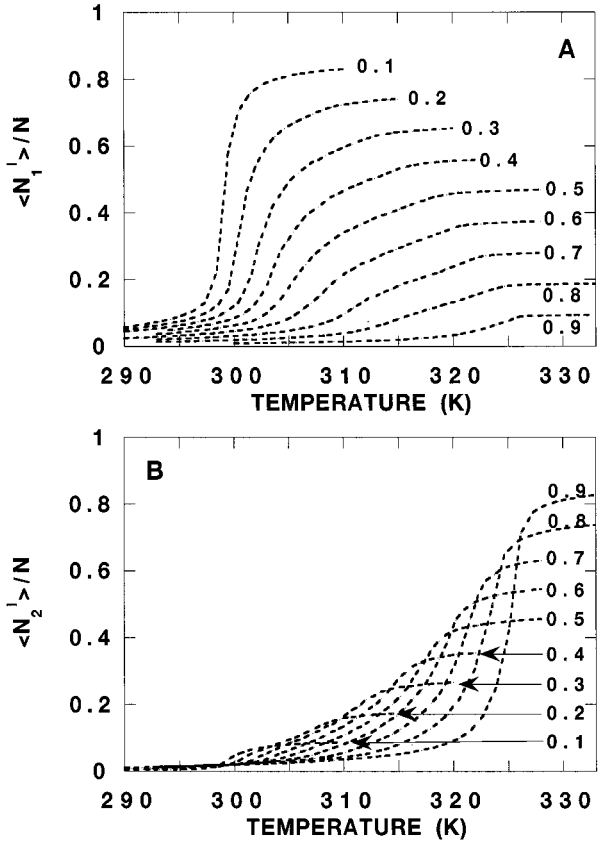

FIGURE 3 Melting curves of the components in different DMPC/DSPC mixtures. (*A*) Calculated $\langle N_1^l(T)\rangle/N$ and (*B*) $\langle N_2^l(T)\rangle/N$ curves. Each curve is labeled by the respective DSPC mole fraction $X_2(= N_2/N)$.

DSPC binary mixture, at any given temperature, X_2^g and X_2^l are increasing functions of the total mole fraction, X_2 (Fig. 5), i.e. there are no horizontal sections of these functions, and thus the lever rule, at best, is only approximately valid.

Cluster statistics

The snapshots were analyzed after every Monte Carlo cycle using a cluster counting algorithm (Stauffer, 1985; Sugar et al., 1994) to obtain the cluster size distributions, cluster numbers, and percolation frequencies.

Fig. 6 shows the size distributions of gel clusters at three different temperatures. The size distribution of the gel clusters is unimodal (×) above the percolation thresholds temperatures of the gel clusters, T_{perc}^{g}. These temperatures, at different mole fractions, are listed in Table 4. Above the percolation threshold temperature, the bilayer contains only small clusters. Large, gel clusters appear in the bilayer below the percolation threshold temperature (● and ○) and the cluster size distribution is bimodal.

The situation is just the opposite for the size distribution of fluid clusters (results are not shown). Below the percolation threshold temperature of fluid clusters, T_{perc}^{l} (Table 4), the size distribution is unimodal with a peak at small cluster size. Above the percolation temperature, however, an additional peak appears at large cluster sizes, i.e., the cluster size distribution becomes bimodal.

The integral of the size distribution provides the average number of clusters in the lattice. In Fig. 7, the average numbers of gel and fluid clusters are plotted against the temperature. With decreasing temperature, the number of gel clusters increases up to a maximum, at 322 K. Below this temperature, the number of gel clusters starts to decrease because the clusters coalesce forming eventually a large gel cluster. With increasing temperature, the number of fluid clusters increases to a maximum at 302 K. Above this temperature, the coalescence of fluid clusters dominate over cluster formation and the number of clusters starts to decrease. It should be noted that, at temperatures at which it is generally assumed that the system exists in a single structural state (e.g., 280 K for the gel and 350 K for the

TABLE 3 Calculated characteristic temperatures of gel-to-fluid transitions in DMPC/DSPC bilayers at different DSPC mole fractions, X_2

X_2*	0.0	0.1	0.2	0.3	0.4	0.5	0.6	0.7	0.8	0.9	1.0
T_{peak1}	297.04	298.9	300.2	302.3	303.8	304.9	307.8	310.4#	—	—	—
T_{peak2}	—	—	308#	310.4	314.4	316.9	318.9	321.3	324.0	325.6	327.7
$T_{N_1^l}$	297.04	298.6	299.5–300.3§	301.6	303.2	304.6	307.7	310.2	314, 321.9¶	324.0	—
$T_{N_2^l}$	—	298.6	300.3, 307¶	311.0	314.6	316.6	319.4	320.9	323.4	325.0	327.7
$T_{N_{12}^{gg}}$	—	298.6	300.5	301.8	303.1	304.6	307.9	310.1	313.8, 321.9¶	324.43	—
$T_{N_{11}^{gl}}$	297.04	299.4	300.3	302.4	304.2	305.8	308.1	311.0	314.0	320.5	—
$T_{N_{12}^{gl}}$	—	301.2	308.5	310.8–312.0§	315.2	317.3	319.5	321.3	323.6	324.2	—
$T_{N_{21}^{gl}}$	—	300.6	307.5	307.9	310.1	313.2	316.0	318.6	317–321§	322.0	—
$T_{N_{22}^{gl}}$	—	301.6	308.2	311.6	314.7	317.3	319.4	321.5	323.4	325.0	327.7
$T_{N_{12}^{ll}}$	—	298.6	300.3, 306.7¶	311.4	314.6	316.6	319.4	320.9	321.9–323.4§	325.0	—

*T_{peak1}, calculated temperature at the low-temperature peak of the excess heat capacity curve; T_{peak2}, calculated temperature at the high-temperature peak of the excess heat capacity curve; $T_{N_1^l}$, temperature at the steepest melting of DMPC chains; $T_{N_2^l}$, at the steepest melting of DSPC chains; $T_{N_{12}^{gg}}$, at the steepest decrease of $\langle N_{12}^{gg}(T)\rangle$; $T_{N_{11}^{gl}}$ at the maximum of $\langle N_{11}^{gl}(T)\rangle$; $T_{N_{12}^{gl}}$ at the maximum of $\langle N_{12}^{gl}(T)\rangle$; $T_{N_{12}^{lg}}$ at the maximum of $\langle N_{12}^{lg}(T)\rangle$; $T_{N_{22}^{gl}}$ at the maximum of $\langle N_{22}^{gl}(T)\rangle$; and $T_{N_{22}^{ll}}$ at the steepest increase of $\langle N_{12}^{ll}(T)\rangle$.

#Temperatures at shoulders of the excess heat capacity curves.

§When the extremum is broad, the respective temperature range is listed.

¶When the curve has two points of inflection, the respective two temperatures are listed.

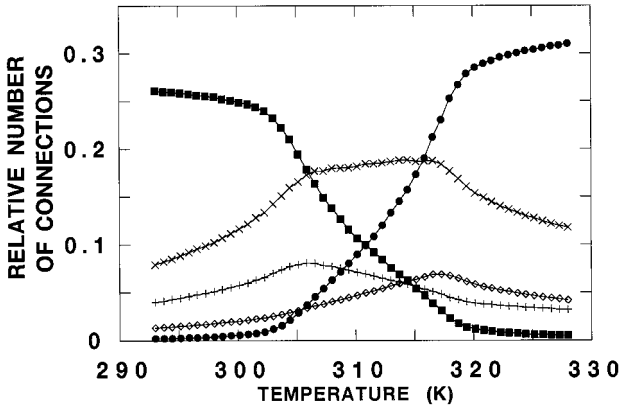

FIGURE 4 Average number of different types of nearest neighbor acyl chains relative to the total number of nearest neighbors. ■, $\langle N^{gg}_{12}(T)\rangle/3N$; +, $\langle N^{gl}_{11}(T)\rangle/3N$; ◇, $\langle N^{gl}_{22}(T)\rangle/3N$; ●, $\langle N^{ll}_{12}(T)\rangle/3N$; ×, the sum of the following averages: $\langle N^{gl}_{12}(T)\rangle$, $\langle N^{gl}_{21}(T)\rangle$, $\langle N^{gl}_{22}(T)\rangle$, and $\langle N^{gl}_{11}(T)\rangle)/3N$, which should be directly proportional to the length of the gel–fluid interface in the bilayer. DMPC/DSPC mixing ratio is 50/50.

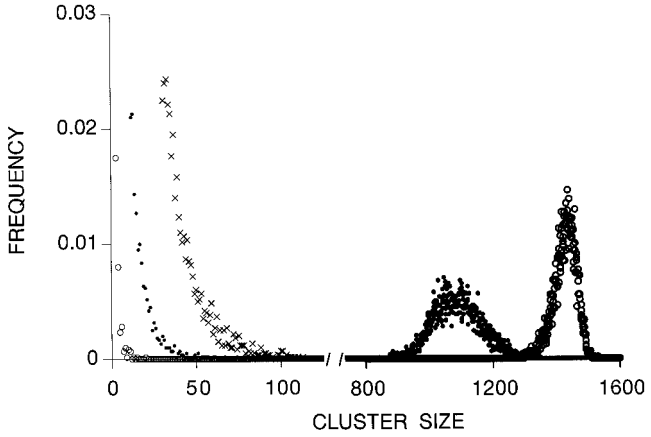

FIGURE 6 Size distributions of gel clusters. The DMPC/DSPC mixing ratio is 50/50 and the lattice size is 40 × 40. The distributions are calculated at the following temperatures: 320.86 K (×), 306.57 K (●), and 302 K (○). The cluster size is the number of acyl chains in a cluster. The frequency is the average number of clusters of a certain size in the lattice.

fluid state), the average number of clusters of the minor component is still significant. This is indicative of lateral density heterogenities existing far from the transition range.

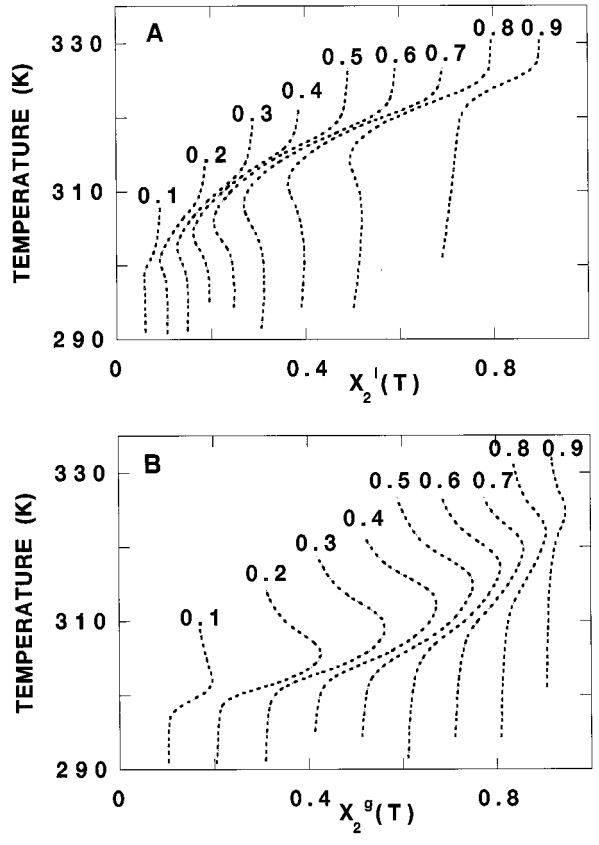

FIGURE 5 DSPC mole fractions in the gel and fluid regions. The *dotted lines* were calculated from the melting curves in Fig. 3 *A* and *B* by means of Eqs. 10 and 11. Each curve is labeled by the respective total DSPC mole fraction $X_2(= N_2/N)$.

When the cluster size distribution is bimodal on the average, there is only one very large cluster in the lattice. A large cluster is percolated if it spans the lattice either from the top to the bottom or from the left to the right edge. The frequency of the appearance of a percolated cluster at the end of each Monte Carlo cycle is the percolation frequency. In Fig. 8 *A*, and *B*, the percolation frequencies of fluid and gel clusters are plotted against the temperature at different mixing ratios. The percolation threshold temperatures of the fluid and gel clusters, T^l_{perc} and T^g_{perc} listed in Table 4 are in good agreement with the peak positions of the excess heat capacity curve T_{peak1} and T_{peak2}, respectively. The temperatures, $T^g_{perc0.36}$, where the percolation frequency of the gel clusters is 0.36, are also listed in Table 4 at different mole

TABLE 4 Calculated and experimental percolation threshold temperatures of the gel-to-fluid transitions in DMPC/DSPC lipid bilayers at different DSPC mole fractions, X_2

X_2*	0.3	0.4	0.5	0.6	0.7
T_{peak1}	302.3	303.8	304.9	307.8	310.4#
T_{peak2}	310.4	314.4	316.9	318.9	321.3
T^l_{perc}	300.8	302.2	303.9	308.5	313.1
T^g_{perc}	309.1	313.8	317.5	320.6	323.0
$T^g_{perc0.36}$	307.1	311.9	315.9	318.9	321.5
T_{FRAP}	306.6	312.0	316.0	319.0	321.5

The determination of the percolation threshold temperature is similar to that of the completion temperature of the transition (see the legend to Fig. 1). A straight line is fitted to the inflection point of the percolation frequency curve (Fig. 8) and its intercept with the zero frequency line defines the percolation threshold temperature.

*T_{peak1}, calculated temperature at the low-temperature peak of the excess heat capacity curve; T_{peak2}, calculated temperature at the high-temperature peak of the excess heat capacity curve; T^l_{perc}, calculated percolation threshold temperature of fluid clusters; T^g_{perc}, calculated percolation threshold temperature of gel clusters; $T^g_{perc0.36}$, temperature at which the percolation frequency of gel clusters is 0.36; T_{FRAP}, threshold temperature from the FRAP experiment (Vaz et al., 1989).

#Temperatures at shoulders of the excess heat capacity curves.

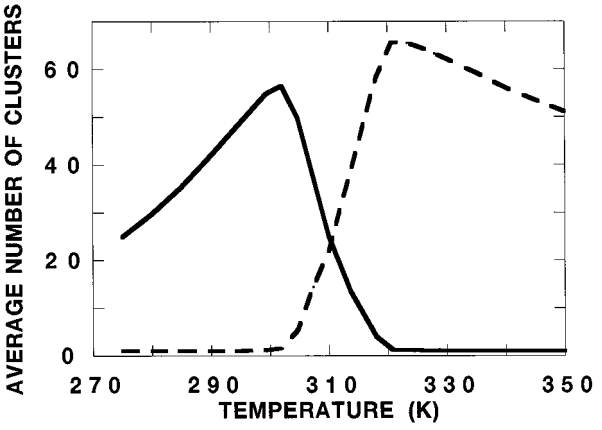

FIGURE 7 Average number of gel and fluid clusters. DMPC/DSPC mixing ratio is 50/50 and the lattice size is 40 × 40. *Solid line,* fluid clusters; *dashed line,* gel clusters.

fractions. $T^{g}_{perc0.36}$ is in excellent agreement with the threshold temperature, T_{FRAP}, obtained from FRAP experiments (Vaz et al., 1989) at mole fractions from 0.3 to 0.7 (Fig. 8 *D*).

Although the percolation threshold temperature depends on both the mixing ratio and the state of the clusters (Table 4), the percolation threshold mole fraction is independent of these factors. This is demonstrated in Fig. 8 *C* where the percolation frequency curves of Fig. 8 *B* are replotted showing the percolation frequencies against the mole fraction of gel lipid. From Fig. 8 *C*, the percolation threshold mole fraction of gel lipid is 0.24. At a percolation frequency of 0.36, which is the percolation frequency at the FRAP threshold temperatures, the mole fraction of the gel lipid is 0.34. If the results in Fig. 8 *A* are plotted against the mole fraction of fluid lipid, a curve identical to Fig. 8 *C* is obtained (results are not shown) and thus the percolation threshold of the fluid clusters is at a mole fraction of fluid lipid of 0.24. We note that, in agreement with the exact results of the percolation theory (Stauffer, 1985), the percolation threshold mole fraction is 0.5 when the chains are not chemically connected and every w^{kl}_{ij} parameter is equal to zero. In summary, the percolation threshold mole fraction of gel or fluid lipid depends on molecular properties such as packing geometry and interchain interactions, whereas it is independent of thermodynamic properties such as tempera-

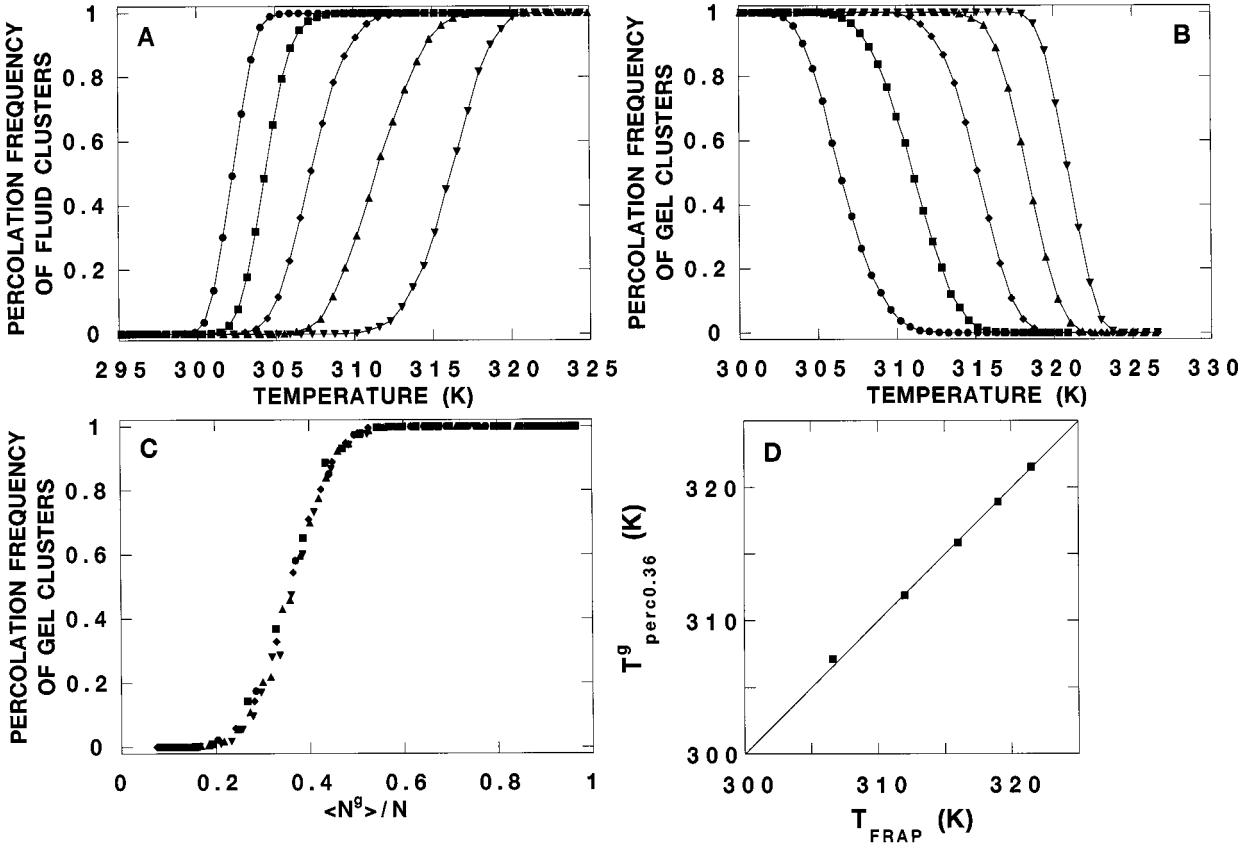

FIGURE 8 Percolation frequency of gel and fluid clusters in DMPC/DSPC mixtures. (*A*) Calculated percolation frequency of fluid clusters versus temperature. (*B*) Calculated percolation frequency of gel clusters versus temperature. (*C*) Calculated percolation frequency of gel clusters versus mole fraction of gel lipid $\langle N^g \rangle / N$. DMPC/DSPC mixing ratios are: 70/30 (●), 60/40 (■), 50/50 (◆), 40/60 (▲) 30/70 (▼). (*D*) Temperatures at 0.36 percolation frequency of gel clusters are plotted against the threshold temperatures obtained from FRAP experiments at different mole fractions. The slope of the regression line is 1.00 ± 0.02, whereas the linear correlation coefficient is $r = 0.9994$.

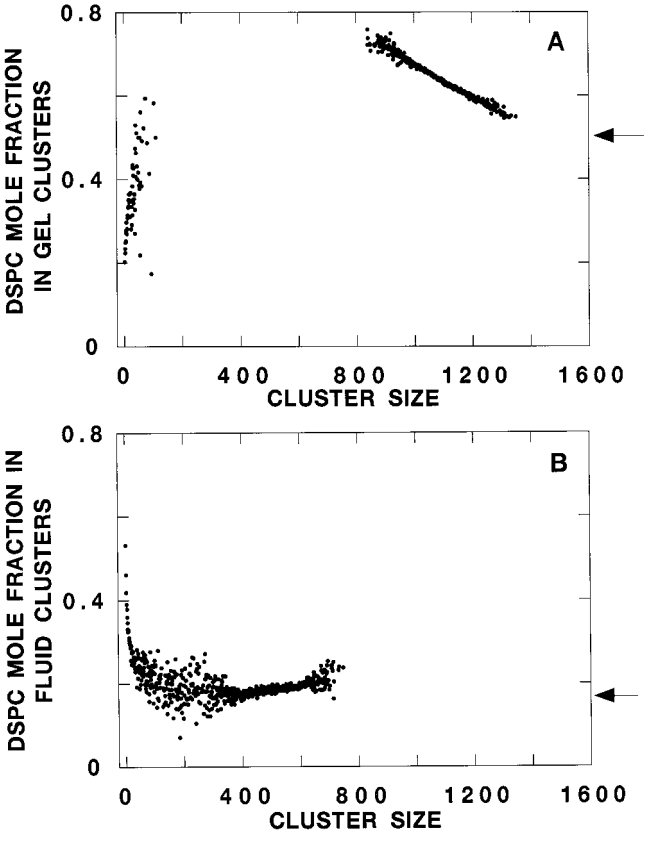

FIGURE 9 Average mole fraction of DSPC in gel and fluid clusters of different sizes. DMPC/DSPC mixing ratio is 50/50 and the lattice size is 40 × 40. Average DSPC mole fraction versus cluster size was calculated at 306.57 K (●). (*A*) DSPC mole fraction in gel clusters. (*B*) DSPC mole fraction in fluid clusters. *Arrows* at the vertical axis mark the mole fractions, X_2^g and X_2^l in the gel and fluid state regions, respectively.

ture, system composition, and the state of the percolating cluster.

The average size of the small gel and fluid state clusters exhibit a maximum at their respective percolation threshold temperature, T^g_{perc} and T^l_{perc} (results not shown). At a mixing ratio of 50/50, the average size of the small gel and fluid clusters is in the range from zero to six chains. However, the size distribution of small clusters is rather broad, especially at the percolation threshold temperatures. Approaching the percolation threshold, the average size of the large cluster linearly decreases and, at the percolation threshold temperature, the large cluster ceases to exist. The linear relationship between temperature and the average size of the large cluster breaks down at cluster sizes comparable with the lattice size, e.g., at a mixing ratio of 50/50, the linear relationship breaks down at about 303 K and 317 K for the large gel and fluid cluster, respectively.

It is important to mention that both the cluster size and cluster number increase with the lattice size but we will not discuss these scaling properties here. However, at infinite lattice size, the initial tail of the percolation frequency curves disappears and the slope of the curves becomes discontinuous at the percolation threshold (Stauffer, 1985).

The average mole fraction of DSPC acyl chains in gel and fluid clusters is plotted against the cluster size in Fig. 9 *A*, and *B*, respectively. For comparison, the DSPC mole fraction in the gel and fluid state region, X_2^g and X_2^l, is marked by an arrow on the vertical axis of the figures. (Although the quantitative aspects of the DSPC mole fraction as a function of gel cluster size will depend on lattice size, the qualitative feature of the result depicted in Fig. 9 *A* should be independent of lattice size. For example, with increasing lattice size, the peak position will increase.) In small gel clusters, the DSPC mole fraction increases with increasing cluster size, whereas it decreases in the large gel clusters with increasing cluster size (Fig. 9 *A*). However, in small fluid clusters, the DSPC mole fraction decreases with increasing cluster size, but it increases in the large, fluid clusters with increasing cluster size (Fig. 9 *B*). These characteristic cluster size dependences are related to the inhomogeneous distribution of the components in the different cluster types.

The inhomogeneous distribution of the components in the gel and fluid clusters

One can classify acyl chains forming a gel or fluid cluster as either inner or peripheral chains. An inner chain is surrounded exclusively by acyl chains of the same cluster, whereas, among the nearest neighbors of a peripheral chain, there is at least one acyl chain that is not an element of the cluster. The largest gel and fluid clusters were analyzed at the end of each Monte Carlo cycle to determine the number of inner and peripheral points of the cluster (C^i and C^p, respectively), and the number of DSPC chains among the inner and peripheral points (C_2^i and C_2^p, respectively). The

TABLE 5 Average compositions in the inner and peripheral points of the largest gel and fluid clusters

Phase	Gel			Fluid		
Temperature* (K)	306.6	315.1	320.9	306.6	315.1	320.9
$\langle C\rangle$	1088 ± 75	481 ± 77	28 ± 15	502 ± 84	1106 ± 67	1440 ± 26
$\langle C^i/C\rangle$	0.60 ± 0.03	0.48 ± 0.08	0.14 ± 0.46	0.45 ± 0.09	0.57 ± 0.03	0.66 ± 0.006
$\langle C_2^p/C^p\rangle$	0.53 ± 0.15	0.73 ± 0.39	0.74 ± 0.84	0.22 ± 0.12	0.43 ± 0.16	0.51 ± 0.11
$\langle C_2/C\rangle$	0.64 ± 0.05	0.81 ± 0.18	0.76 ± 0.65	0.19 ± 0.06	0.39 ± 0.05	0.49 ± 0.02
$\langle C_2^i/C^i\rangle$	0.71 ± 0.09	0.89 ± 0.27	0.88 ± 1.27	0.15 ± 0.06	0.35 ± 0.07	0.47 ± 0.05

The standard deviation of 6000 data is shown. The standard error of the mean is S.D./$\sqrt{6000}$.

*C ($= C^i + C^p$), the number of chains in the largest cluster; C_2 ($= C_2^i + C_2^p$), the number of DSPC chains in the largest cluster.

averages and standard deviations obtained from the analysis of 6000 snapshots of a 50/50 DMPC/DSPC mixture of three different temperatures are listed in Table 5. This analysis shows that the mole fraction of DSPC acyl chains is significantly larger inside than at the periphery of the gel clusters (Table 5). This nonuniform distribution of the components explains the cluster size dependence of cluster composition. As the gel cluster grows, the perimeter-to-area ratio decreases, resulting in an increase in the mole fraction of DSPC chains in the gel cluster. At some maximum size, the number of DSPC molecules available to cluster growth will become limiting and any further growth be dominated by condensation of DMPC molecules onto the cluster. This will result in a reduction of the mole fraction of DSPC chains in the gel cluster. The converse is true for the growth of fluid clusters.

The physical reason for the inhomogeneous distribution of the components in the gel and fluid clusters is in the nonideality of the DMPC/DSPC mixture. Random distributions can be achieved only when every w_{ij}^{kl} parameter is zero. Note that Jørgensen et al. (1993, 1996), using a 10-state model, simulated the lateral distribution of the components in DMPC/DSPC mixtures. These authors described a similar inhomogeneous distribution of the components in the gel clusters. Also, in agreement with our above conclusion, they note that the inhomogenity becomes more pronounced as the degree of nonideal mixing increases.

CONCLUSIONS

A simple two-component, two-state lattice model is sufficient to simulate the excess heat capacity curves of DMPC/DSPC mixtures in quantitative agreement with the observed data. At every DMPC/DSPC mole fraction investigated, the temperature-induced gel–fluid transition appears to be a continuous transition in the thermodynamic limit. The temperature characteristics of the configurational properties, such as the percolation threshold temperatures or temperatures at the steepest melting of the bilayer components, correlate well with the temperatures at the maxima of the excess heat capacity curves rather than with the onset and completion temperatures of the gel–fluid transition. In the gel–fluid coexistence region, we also found excellent agreement between the threshold temperatures at different system compositions detected in FRAP experiments and the temperatures at which the percolation probability of the gel clusters is 0.36.

APPENDIX

In the case of a one-component bilayer, the partition function can be obtained in the following closed form if parameter $w^{gl} = 0$,

$$Q(T, N) = [1 + q]^N, \tag{A1}$$

where $q = e^{-(\Delta E - T\Delta S)/kT}$. The excess heat capacity can be calculated from the partition function as

$$C_V = \frac{1}{kT^2}\frac{\partial^2 \ln Q}{\partial(1/kT)^2} = \frac{N\Delta E^2}{kT^2}\frac{q}{(1+q)^2}. \tag{A2}$$

The temperature derivative of C_V is

$$\frac{dC_V}{dT} = \frac{N\Delta E^2}{kT(1+q)^2}\frac{dq}{dT}\left\{-\frac{2k}{\Delta E} + \frac{1-q}{1+q}\frac{1}{T}\right\}. \tag{A3}$$

The factor in the braces becomes zero at the maximum of the excess heat capacity (i.e., at temperature T_m) and thus ΔS satisfies

$$\frac{\Delta S}{k} = \frac{\Delta E}{kT_m} + \ln\frac{1 - 2kT_m/\Delta E}{1 + 2kT_m/\Delta E}. \tag{A4}$$

Equation A4 can be further simplified if $1 \gg 2kT_m/\Delta E$ and then

$$\Delta S \approx \frac{\Delta E}{T_m}. \tag{A5}$$

By using the above approximation, instead of Eq. A4, in estimating ΔS for DSPC lipid bilayer, with T_m = 327.78 K and ΔE = 5,250 cal/mol-chain, the above approximation results in an error of 3%.

We would like to thank Dr. Barbora Piknova, Dr. Anne K. Hinderliter, Dr. Thomas Heimburg, and Mr. Kim Thompson for providing the excess heat capacity data, and to Dr. David S. Cafiso for running pilot NMR experiments to determine the differences in dipole potential between fluid and gel state regions.

Dr. Sugar acknowledges Mrs. Lawrence Garner's generous support. The work was supported by NIH grants GM23573 and GM37658 and NSF grant MCB 9632095.

REFERENCES

Brumbaugh, E. E., M. L. Johnson, and C. Huang. 1990. Non-linear least squares analysis of phase diagrams for non-ideal binary mixtures of phospholipids. *Chem. Phys. Lipids.* 52:69–78.

Brumbaugh, E. E. and C. Huang. 1992. Parameter estimation in binary mixtures of phospholipids. *Meth. Enzymol.* 210:521–539.

Brumm, T., K. Jørgensen, O. G. Mouritsen, and T. M. Bayerl. 1996. The effect of increasing membrane curvature on the phase transition and mixing behavior of a dimyristoyl-sn-glycero-3-phosphatidylcholine/distearoyl-sn-glycero-3-phosphatidylcholine lipid mixture as studied by Fourier transform infrared spectroscopy and differential scanning calorimetry. *Biophys. J.* 70:1373–1379.

Clerc, S. G., and T. E. Thompson. 1995. Permeability of dimyristoyl phosphatidylcholine/dipalmitoyl phosphatidylcholine bilayer membranes with coexisting gel and liquid-crystalline phases. *Biophys. J.* 68:2333–2341.

Cruzeiro-Hansson, L., and O. G. Mouritsen. 1988. Passive ion permeability of lipid membranes modelled via lipid-domain interfacial area. *Biochim. Biophys. Acta.* 944:63–72.

Ferrenberg, A. M., and R. H. Swendsen. 1988. New Monte Carlo technique for studying phase transitions. *Phys. Rev. Lett.* 61:2635–2638.

Glauber, R. J. 1963. Time-dependent statistics of the Ising model. *J. Math. Phys.* 4:294–307.

Heimburg, T., and D. Marsh. 1996. Thermodynamics of the interaction of proteins with lipid membranes. *In* Biological Membranes. A Molecular Perspective from Computation and Experiment. K. M. Merz and B. Roux, editors. Birkhauser, Boston. 405–462.

Huang, K. 1963. *In* Statistical Mechanics. Wiley, New York. 336.

Ipsen, J. H., and O. G. Mouritsen. 1988. Modeling the phase equilibria in two-component membranes of phospholipids with different acyl-chain lengths. *Biochim. Biophys. Acta.* 944:121–134.

Jan, N., T. Lookman, and D. A. Pink. 1984. On computer simulation methods used to study models of two-component lipid bilayers. *Biochemistry.* 23:3227–3231.

Jerala, R., P. F. F. Almeida, and R. L. Biltonen. 1996. Simulation of the gel–fluid transition in a membrane composed of lipids with two connected acyl chains: application of a dimer-move step. *Biophys. J.* 71: 609–615.

Jørgensen, K., M. M. Sperotto, O. G. Mouritsen, J. H. Ipsen, and M. J. Zuckermann. 1993. Phase equilibria and local structure in binary lipid bilayers. *Biochim. Biophys. Acta.* 1152:135–145.

Jørgensen, K., A. Klinger, M. Braiman, and R. L. Biltonen. 1996. Slow nonequilibrium dynamical rearrangement of the lateral structure of a lipid membrane. *J. Phys. Chem.* 100:2766–2769.

Kawasaki, K. 1972. *In* Phase Transitions and Critical Phenomena. Vol. 2, C. Domb and M. S. Green, editors. Academic Press, London. 443.

Knoll, W., K. Ibel, and E. Sackmann. 1981. Small-angle neutron scattering study of lipid phase diagrams by the contrast variation method. *Biochemistry.* 20:6379–6383.

Lu, D., I. Vavasour, and M. R. Morrow. 1995. Smoothed acyl chain orientational order parameter profiles in dimyristoylphosphatidylcholine–distearoylphosphatidylcholine mixtures: a ^{2}H-NMR study. *Biophys. J.* 68:574–583.

Mabrey, S., and J. M. Sturtevant. 1976. Investigation of phase transitions of lipids and lipid mixtures by high sensitivity differential scanning calorimetry. *Proc. Natl. Acad. Sci. USA* 73:3862–3866.

Marsh, D., A. Watts, and P. F. Knowles. 1976. Evidence of phase boundary lipids. Permeability of tempo-choline into dimyristoyl phosphatidylcholine vesicles at the phase temperature. *Biochim. Biophys. Acta.* 458: 161–168.

Mendelsohn, R., and J. Maisano. 1978. Use of deuterated phospholipids in Raman spectroscopic studies of membrane structure. I. Multilayers of dimyristoylphosphatidylcholine (and its d_{54} derivative) with distearoylphosphatidylcholine. *Biochim. Biophys. Acta.* 506:192–201.

Mezei, M., and D. L. Beveridge. 1986. Free energy simulations. *Ann. N.Y. Acad. Sci.* 482:1–23.

Pedersen, S., K. Jørgensen, T. R. Boekmark, and O. Mouritsen. 1996. Indirect evidence for lipid-domain formation in the transition region of phospholipid bilayers by two-probe fluorescence energy transfer. *Biophys. J.* 71:554–560.

Piknova, B., D. Marsh, and T. E. Thompson. 1996. Fluorescence-quenching study of percolation and compartmentalization in two-phase lipid bilayers. *Biophys. J.* 71:892–897.

Priest, R. 1980. Landau phenomenological theory of one and two component phospholipid bilayers. *Mol. Cryst. Liq. Cryst.* 60:167–184.

Risbo, J., M. Sperotto, and O. G. Mouritsen. 1995. Theory of phase equilibria and critical mixing points in binary lipid membranes. *J. Chem. Phys.* 103:3643–3656.

Sankaram, M. B., and T. E. Thompson. 1992. Deuterium magnetic resonance study of phase equilibria and membrane thickness in binary phospholipid mixed bilayers. *Biochemistry.* 31:8258–8268.

Sankaram, M. B., D. Marsh, and T. E. Thompson. 1992. Determination of fluid and gel domain sizes in two-component, two-phase lipid bilayers. An electron spin resonance spin label study. *Biophys. J.* 63:340–349.

Schram, V., H.-N. Lin, and T. E. Thompson. 1996. Topology of gel-phase domains and lipid mixing properties in phase-separated two-component phosphatidylcholine bilayers. *Biophys. J.* 71:1811–1822.

Stauffer, D. 1985. *In* Introduction to Percolation Theory. Taylor and Francis, London and Philadelphia. 110.

Sugar, I. P., R. L. Biltonen, and N. Mitchard. 1994. Monte Carlo simulation of membranes: phase transition of small unilamellar dipalmitoylphosphatidylcholine vesicles. *Meth. Enzymol.* 240:569–593.

Sugar, I. P., and G. Monticelli. 1985. Interrelationships between the phase diagrams of the two-component phospholipid bilayers. *Biophys. J.* 48: 283–288.

Sun, H., and I. P. Sugar. 1997. Acceleration of convergence to the thermodynamic equilibrium by introducing shuffling operations to the Metropolis algorithm of Monte Carlo simulations. *J. Phys. Chem.* 101: 3221–3227.

Suurkuusk, J., B. R. Lentz, Y. Barenholz, R. Biltonen, and T. E. Thompson. 1976. A calorimetric and fluorescent probe study of the gel–liquid crystalline phase transition in small, single-lamellar dipamitoylphosphatidylcholine vesicles. *Biochemistry.* 15:1393–1401.

Van Dijck, P. W. M., A. J. Kaper, H. A. J. Oonk, and J. De Gier. 1977. Miscibility properties of binary phosphatidylcholine mixtures. *Biochim. Biophys. Acta.* 470:58–69.

Vaz, W. L. C., E. C. C. Melo, and T. E. Thompson. 1989. Translational diffusion and fluid domain connectivity in a two-component, two-phase phospholipid bilayer. *Biophys. J.* 56:869–876.

Von Dreele, P. H. 1978. Estimation of lateral species separation from phase transitions in nonideal two-dimensional lipid mixtures. *Biochemistry.* 17:3939–3943.

Wilkinson, D. A., and J. F. Nagle. 1979. Dilatometric study of binary mixtures of phosphatidylcholines. *Biochemistry.* 18:4244–4249.

Wimley, W. C., and T. E. Thompson. 1990. Exchange and flip-flop of dimyristoylphosphatidylcholine in liquid-crystalline, gel and two-component two-phase large unilamellar vesicles. *Biochemistry.* 29: 1296–1303.

Wimley, W. C., and T. E. Thompson. 1991. Transbilayer and interbilayer phospholipid exchange in dimyristoylphosphatidylcholine/dimyristoylphosphatidylethanolamine large unilamellar vesicles. *Biochemistry.* 30:1702–1709.